COMMISSIONING OF THE NEPTUNE PHOTOINJECTOR*

S. G. Anderson, J. B. Rosenzweig, R. Augustsson, S. Boucher, A. Burke, J. England,
M. Loh, P. Musumeci, H. Suk, M. C. Thompson, UCLA Department of Physics and Astronomy,
Los Angeles, CA 90095
C. Clayton, UCLA Department of Electrical Engineering, Los Angeles, CA 90095

Abstract

The status of the rf photoinjector in the Neptune advanced accelerator laboratory is discussed. The components of the photoinjector: the rf gun and booster linac, chicane compressor, and beam diagnostic systems are described. Measurement techniques used to diagnose the short pulse length, high brightness beam are detailed and measurements of emittance and pulse compression are given. The effect of the pulse compressor on transverse emittance is explored.

1 THE NEPTUNE LABORATORY

The mission of the Neptune Advanced Accelerator Laboratory is to accelerate a high quality electron beam in a plasma beat-wave accelerator, while preserving the phase space density of the beam. [1] To that end, the laboratory consists of two major components; the rf photoinjector, and the high power, short pulse, two-frequency Mars CO_2 laser. [2] In addition to the plasma beat wave accelerator (PBWA), other advanced accelerator experiments such as plasma wake-field acceleration [3], plasma lens, and inverse free-electron laser acceleration [4] are planned. In addition to advanced accelerator experiments, the photoinjector allows the study of high brightness beam physics, including the process of emittance growth in bends, which will be detailed in this paper.

2 THE PHOTOINJECTOR

The Neptune photoinjector has many components, the most important of which are described here. The accelerator is a split system consisting of a photocathode gun, a drift space, and a booster linac. The gun was produced by a BNL-SLAC-UCLA collaboration. [5] It is a 1.625 cell π-mode standing wave cavity which is typically run with a peak accelerating field of 85 MV/m. The booster linac is located approximately one meter down-stream of the gun. The structure is a 7 and 2/2 cell π-mode standing wave plane-wave-transformer (PWT.) The PWT benefits from strong cell-to-cell coupling and large mode separation which allows it to have only the accelerating mode resonant in the required fill time (4 μsec.) [6] The beam energy after the PWT is typically 12 MeV.

The electron beam can be compressed in the photoinjector using the chicane magnets. The compressor is a set of four dipole magnets that can be used either to compress the beam or by switching magnet polarities, as a spectrometer. When run as a compressor, the magnets produce a shorter path length for electrons of higher energy. This property is utilized by running the beam through the PWT ahead of peak accelerating phase, giving the proper correlation in the longitudinal phase space of the beam.

There are a number of diagnostics distributed throughout the beamline. The main devices that aid in beam transport, and measure spot size and profile are pop-in YAG screens. The YAG screens employed at Neptune consist of Ce doped YAG crystals that are 0.5 mm thick and range in diameter from 1 to 2.5 cm. Each crystal is mounted on a remotely controlled pneumatic actuator. A mirror is mounted directly behind each crystal at 45° directing the light produced by the YAG screen out of vacuum through a window and into a video camera. The video data is then displayed in the control room and can be digitized for real-time computer-automated calculations, or saved for latter analysis.

An integrating current transformer (ICT) is used to measure beam charge. The key advantages of the ICT are that measurements are single-shot and non-destructive. This allows us to measure charge simultaneously with a destructive diagnostic such as emittance or pulse length. The single-shot nature of the diagnostic is especially useful because it allows the shot-to-shot fluctuations in beam charge to be factored out of measurements where space-charge is an important effect.

3 BEAM DIAGNOSTICS

The two main diagnostics we use at Neptune to measure beam quality are the emittance slits [7], and the coherent transition radiation (CTR) based pulse length measurement. [8] Each diagnostic is described in detail below.

3.1 Slit-Based Emittance Measurements

In this emittance measurement system the beam is collimated by a set of slits (one dimensional pepper pot.) The collimated beamlets then drift a given length to a YAG screen where the image can be captured and

* Work supported by U.S. Dept. of Energy grant DE-FG03-92ER40693.

analyzed. The slits serve two purposes. The first is to create beamlets that will expand in the drift space due to the thermal emittance of the beamlet and not due to the space-charge forces in it. This is opposed to the behavior of the full beam, which is dominated by space charge forces. The relative strength of these forces can be evaluated by taking the ratio of the forcing terms in the RMS envelope equation.

$$\sigma_x'' = \frac{\varepsilon_n^2}{\gamma^2 \sigma_x^3} + \frac{2I}{\gamma^3 I_0 (\sigma_x + \sigma_y)} \quad (1)$$

The ratio for the full beam is simply:

$$R = \frac{I\sigma_0^2}{I_0 \gamma \varepsilon_n^2} \quad (2)$$

For typical Neptune parameters, R>>1, indicating a space charge dominated beam. For a beamlet, however, this ratio becomes:

$$R_{beamlet} = \sqrt{\frac{2}{3\pi}} \frac{I}{\gamma I_0} \left(\frac{d}{\varepsilon_n} \right)^2 \quad (3)$$

Where d is the slit width (50 μm in this case.) This ratio is typically on the order of 10^{-2}, indicating emittance dominated beamlets.

The second duty of the slits is to provide a way to extract the horizontal phase space of the original beam. Since the slit separation is known, the number of slits illuminated gives the size of the beam on the slits. The position and width of each beamlet on the screen combined with the length of the drift give the beamlets average momentum and momentum spread.

The slit-based system has been used at Neptune to measure normalized, horizontal emittances from 5 to 25 mm mrad.

3.2 CTR Based Pulse Length Diagnostic

The basic idea behind this device is that the coherent portion of the transition radiation produced when the beam hits a thin foil has the same frequency spectrum as the beam. Therefore, by autocorrelating the CTR, we gain information about the longitudinal profile of the beam. In our diagnostic, the beam hits a thin foil mounted at 45°. The back scattered CTR moves out of the vacuum through a quartz window and is collected by a parabolic mirror. A transmission wire grid of 100 micron spacing then splits the radiation. Half of the signal is sent to a reference detector while the remainder goes into a Michelson-type interferometer. The light that propagates through the interferometer is then sent to a second detector and the ratio of the two detector signals is measured as a function of the length of the interferometer delay arm.

This diagnostic has produces measurements of pulse lengths down to 0.5 picoseconds with the beam compressed. Figure 1 shows a typical example of data obtained with the interferometer.

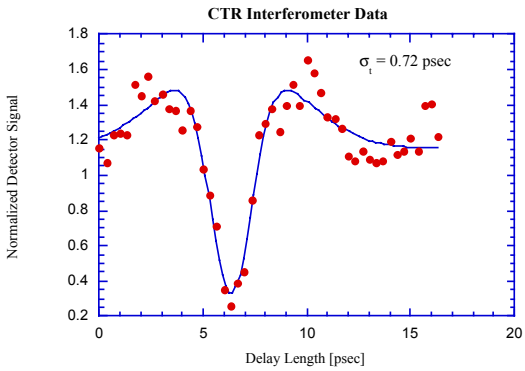

Figure 1: Pulse length data taken using the CTR diagnostic. The solid line is a fit function that yields the bunch length. In this case the chicane was used to compress the beam from 4 to 0.7 picoseconds rms.

4 EMITTANCE GROWTH IN THE COMPRESSOR

With the pulse length diagnostic and transverse phase space reconstruction of the beam, we have examined the evolution of the beam in the compressor.

4.1 Experimental Procedure and Results

In the measurement described here, the beam was compressed by varying the injection phase in the PWT. This phase was monitored by mixing the low-level rf with the signal from an rf probe in the PWT. The compressor magnets were first set in a spectrometer configuration, in order to determine the proper field values to produce a 22.5° bend angle, and to record the PWT phase for optimal beam energy. The magnets were then set to compress and the best phase for compression was found using the CTR diagnostic. At this point the measurement was performed by adjusting the linac phase and taking images of the beam passing through the slits.

The emittance found by reconstructing the phase space for each data point is shown in figure 2.

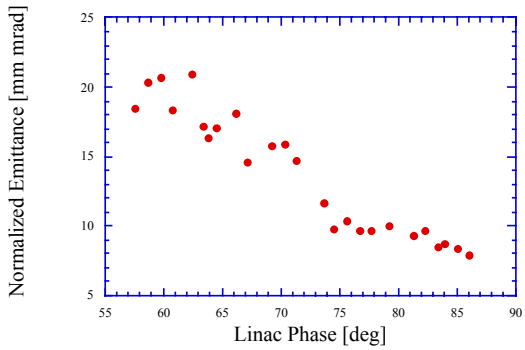

Figure 2: Horizontal emittance versus PWT phase.

Figures 3 and 4 show images of the beam passing through the slits and their phase space reconstructions for

a non-compressing and maximally compressing phase respectively.

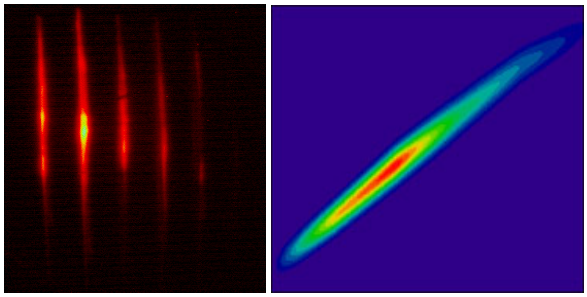

Figure 3: Slit image and transverse phase space reconstruction of the uncompressed beam.

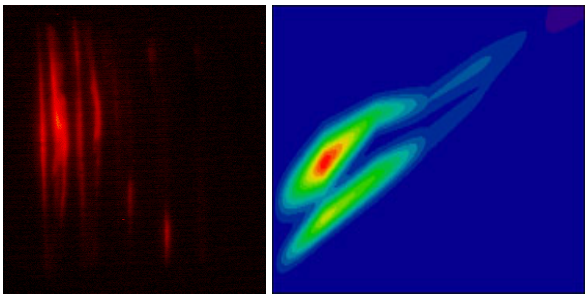

Figure 4: Slit image and transverse phase space reconstruction of the compressed beam.

We see that in the case of the compressed beam, the transverse phase space bifurcates. This behavior is evident in the beam images as we see that more that one beamlet emerges from each slit.

4.2 Analysis

In order to understand which physical processes (velocity field or acceleration field related) are contributing to the emittance growth and phase space bifurcation seen in this measurement, a number of simulation codes are in use. These include TREDI [9], a code based on Lienard-Wiechart potentials, PARMELA [10], used to provide input distributions to TREDI as well as to simulate the compressor using a point-to-point space-charge routine, and elegant [11], which calculates the effects of coherent synchrotron radiation (CSR.)

Initial simulations agree reasonably well with experimental data, and indicate that velocity field effects are responsible for most of the emittance growth in this measurement.

5 REFERENCES

[1] C. Clayton, *et al*., *Nucl. Instr. Methods A* **410** (1998).
[2] C. Clayton, *et al*., *Phys. Rev. Lett*. **54**, 2353 (1985).
[3] H. Suk, *et al*., *Phys. Rev. Lett*. **86**, 1011 (2001).
[4] P. Musumeci, *et al*., these proceedings
[5] D. T. Palmer, *et al*., *Proc. 1997 Particle Accelerator Conf.*, 2846 (IEEE, 1997).
[6] R. Zhang, *et al*., *Proc. 1995 Particle Accelerator Conf*., 1102 (IEEE, 1995).
[7] http://pbpl.physics.ucla.edu/papers/PDF/emitslit.pdf
[8] A. Murokh, *et al*., *Nucl. Instr. Methods A* **410** (1998).
[9] F. Ciocci, *et al*., *Nucl. Inst. Methods A* **393**, 434 (1997).
[10] http://pbpl.physics.ucla.edu/docs/parmela.pdf
[11] M. Borland, "elegant: A Flexible SDDS-Compliant Code for Accelerator Simulation," Advanced Photon Source LS-287, September 2000 http://www.aps.anl.gov/techpub/lsnotes/lsnotesTOC.html